JGR Oceans

RESEARCH ARTICLE
10.1029/2019JC015273

Mesoscale Eddies Observed at the Denmark Strait Sill

Martin Moritz[1,2], Kerstin Jochumsen[2], Ryan P. North[1], Detlef Quadfasel[1], and Héðinn Valdimarsson[3]

[1]Institut für Meereskunde, Universität Hamburg, Hamburg, Germany, [2]Bundesamt für Seeschifffahrt und Hydrographie (BSH), Hamburg, Germany, [3]Marine and Freshwater Research Institute, Reykjavik, Iceland

Key Points:
- Mesoscale flow variability is observed at the Denmark Strait Sill with a five-mooring array
- Trains of alternating eddies are passing the sill
- Anticyclones are found to be related to the occurence of boluses and pulses

Correspondence to:
M. Moritz,
martin.moritz@bsh.de

Citation:
Moritz, M., Jochumsen, K., North, R. P., Quadfasel, D., & Valdimarsson, H. (2019). Mesoscale eddies observed at the Denmark Strait sill. *Journal of Geophysical Research: Oceans*, *124*, 7947–7961. https://doi.org/10.1029/2019JC015273

Received 9 MAY 2019
Accepted 25 SEP 2019
Accepted article online 16 OCT 2019
Published online 19 NOV 2019

Abstract The Denmark Strait overflow is the major export route of dense water from the Arctic Mediterranean into the North Atlantic. At the Strait's shallow sill, the overflow is a bottom-intensified cold and dense plume, bound to the east by a thermal front formed with the warmer, northward flowing North Icelandic Irminger Current. More than two decades of observations at the sill show strong fluctuations of volume flux on daily time scales. To better understand the source of this variability, a five-mooring array was installed at the sill, capturing nearly 1 year of velocity and bottom temperature measurements at a high temporal and spatial resolution. Bottom temperature fluctuations that exceed 4 °C indicate a meandering of the front between the plume and the North Icelandic Irminger Current. Current vector rotation shows trains of alternating cyclones and anticyclones at the sill. An eddy crosses the sill every 3 to 6 days with a mean velocity of 0.4 m/s and a typical diameter of 30 to 40 km. The results suggest that anticyclones, with centers passing through the deepest part of the sill, may be responsible for periods of increased volume flux—also referred to as boluses and pulses in previous studies. Although the relationship between eddies, pulses, and boluses is still unclear, the results show that eddies are directly linked to fluctuations in the strength, thickness, and position of the overflow plume.

Plain Language Summary The southward flow of dense water from the Arctic ocean plays a crucial role in global ocean circulation but is almost immediately constrained on its way south by a submarine ridge that connects Greenland, Iceland, the Faroe Islands, and Scotland. The southward flow is therefore forced to pass through several straits and up and over relatively shallow sills. Most of the flow passes over a sill in the Denmark Strait, located between Greenland and Iceland. In this study, we present observations from an array of instruments, which measure the southward flow as it passes over the Denmark Strait sill. The flow is characterised by trains of eddies (vortices), with an alternating sense of rotation; meaning a counterclockwise eddy is usually followed by a clockwise eddy. The eddies are 30 to 40 km wide and need about 1 day to pass over the sill. These eddies help to explain pronounced changes in the flow across the sill, as they can help either to speed up the flow or slow it down. The results of this study contribute to understanding mesoscale fluctuations, which influence local mixing processes and water mass transports.

1. Introduction

Within the Arctic Mediterranean, the basins known as the Nordic Seas are important areas of water mass transformation and recirculation (e.g., Latarius & Quadfasel, 2016; Pickart & Watts, 1990). Warm water entering the region from the North Atlantic in surface intensified currents loses heat to the atmosphere, thereby increasing its density and reducing its buoyancy (e.g., Mauritzen, 1996). As a consequence, a deep water density difference between the Nordic Seas and the North Atlantic is established, which drives a subsurface southward return flow of dense water (e.g., Hansen et al., 2008). The Greenland-Scotland Ridge acts as a topographic barrier to this return flow, and as a result the dense water is limited to passing through a limited number of gaps and channels. The deepest channels connecting the Nordic Seas and the North Atlantic are the Faroe Bank Channel and the Denmark Strait (DS). Flow through the DS provides the largest source of lower North Atlantic Deep Water (Hansen et al., 2008). The DS has a sill depth of 650 m and is about 100 km wide, which is relatively large compared to the Rossby radius of about 5 km in the Nordic Seas (Nurser & Bacon, 2014).

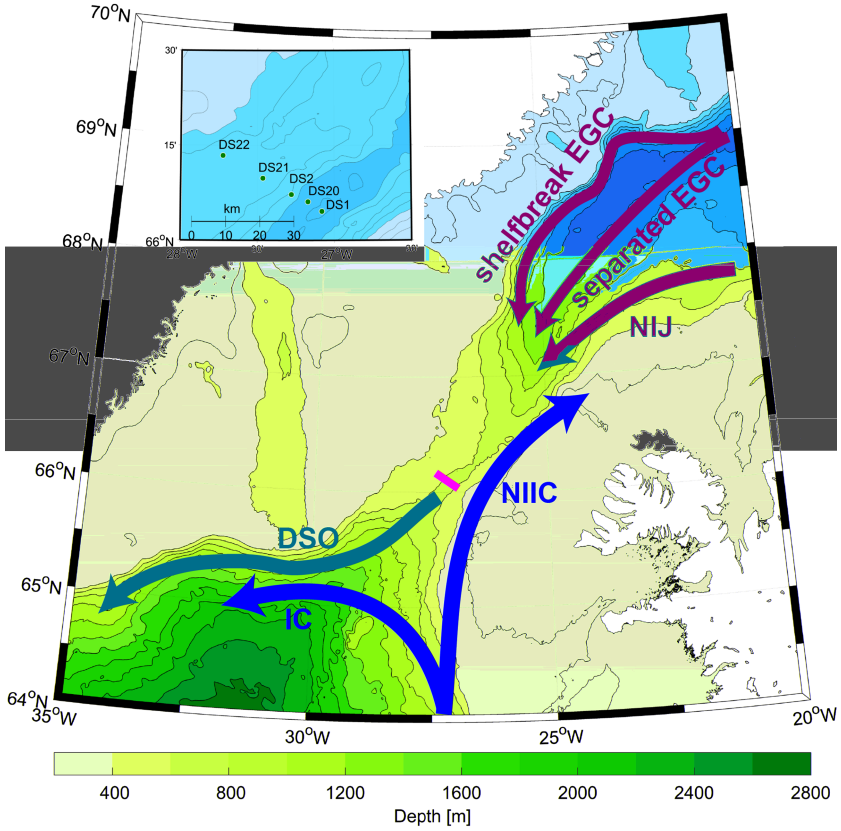

Figure 1. Map of the Denmark Strait and scheme of the mean circulation at 300-m depth. Warm water (red) is transported north-eastward by the North Icelandic Irminger Current (NIIC) and westward by the Irminger Current (IC). The cold and dense water (purple) of the Denmark Strait Overflow (DSO) is supplied by the two branches of the East Greenland Current (EGC) and the North Icelandic Jet (NIJ). The yellow line and the inset show the position of the mooring array at the sill.

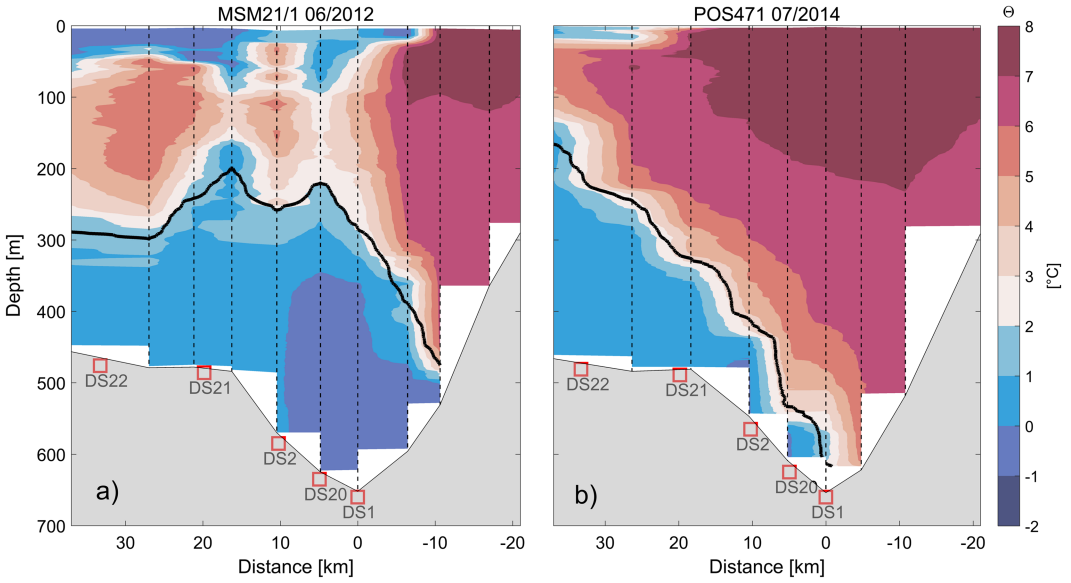

Figure 2. Potential temperature distribution along the Denmark Strait sill during cruises (a) MSM21/1 (2012) and (b) POS471 (2014) from CTD stations marked by vertical dashed lines. The thick black line shows the 27.8 kg/m^3 isopycnal, and the positions of the moorings are indicated by the red squares at the seafloor.

Denmark Strait Overflow Water (DSOW) has several sources that vary in temperature and salinity and also in their volumetric contribution (Mastropole et al., 2017). These sources are the shelf break East Greenland Current, the separated East Greenland Current and the North Icelandic Jet (NIJ), all of which merge within the DS (Figure 1). The resulting bottom-intensified DSOW plume is cold and dense and banked to the western side of the deep channel as it approaches and overflows the sill. To the east, on the western Icelandic shelf, the North Icelandic Irminger Current (NIIC) carries warm water of Atlantic origin north-eastward. Between the NIIC and the DSOW a pronounced thermal front is established (Figure 2).

The flow through the DS has been described as a hydraulically controlled flow through a channel (Käse & Oschlies, 2000; Quadfasel & Käse, 2007), a south-westward directed barotropic jet with a horizontal shear and vorticity gradient (Fristedt et al., 1999), as well as a bottom intensified deep density-driven overflow plume (Macrander et al., 2007). These diverging descriptions highlight the gaps in our understanding of the flow mechanics in the DS. The different views either result from the flow's high variability, which is much higher at the sill than at downstream locations in the North Atlantic (Fischer et al., 2015) or explain different phases of the same instability process. Furthermore, the observed high temporal variability at the DS sill may originate from further upstream or be generated in the vicinity of the sill, due to topographic forcing at the saddle point (Håvik et al., 2017).

The variability of the velocity field and water mass distribution has been analyzed in a number of observational, theoretical, and model studies, which all find strong fluctuations on periods of several days, associated with mesoscale variability (e.g., Jochumsen et al., 2012; Krauss & Käse, 1998; Macrander et al., 2007; Shi et al., 2001; Smith, 1976; Spall & Price, 1998; Worthington, 1969). The longest spanning study used more than 20 years of DSOW volume flux measurements at the sill and found strong variability on time scales of days to years, with most energy below a period of 20 days (Jochumsen et al., 2017). Eddies are one potential source of variability at the sill, and while cyclones and anticyclones are documented north and south of the sill from observations and models, they have not been clearly identified in the passage or at the sill (e.g., Bruce, 1995; Harden et al., 2016; Jungclaus et al., 2001; Krauss & Käse, 1998; Lundrigan & Demirov, 2019; Shi et al., 2001; Voet & Quadfasel, 2010).

Recent observational and model studies describe the variability in terms of a background flow disturbed by boluses or pulses passing over the sill (Almansi et al., 2017; Mastropole et al., 2017; von Appen et al., 2017). Boluses are defined as cold, weakly stratified lenses that are accompanied by increased current speeds and a thickening of the plume. Pulses have an increased flow speed and a thinner plume. Mastropole et al. (2017) conclude that the boluses consist mostly of water that originates from the Iceland Sea and are supplied mainly by the NIJ.

However, most studies at the sill are based solely on measurements of one- to two-moored Acoustic Doppler Current profilers. From August 2014 to June 2015 the mooring array was extended to include five instruments to improve the spatial resolution along the DS sill and to provide a more accurate volume transport estimate (Jochumsen et al., 2017). The resulting data set of 11 months at high temporal resolution is eddy permitting and reveals temperature and velocity fluctuations on daily time scales. We use these data to describe the mesoscale variability in the strait and identify eddies, which are prominent features at the mooring array. The data set is further explored to evaluate the occurrence of boluses and pulses (section 3). Finally, the connection between these two types of mesoscale structures is summarized and discussed (section 4).

2. Data and Methods

2.1. Instruments and Mooring Setup

The mooring array deployed in 2014/2015 consisted of five current meters labeled DS1, DS20, DS2, DS21, and DS22 (from southeast to northwest; Figures 1 and 2). DS1 and DS2 are the long-term moorings maintained by the Marine and Freshwater Research Institute), Reykjavik, Iceland, and the University of Hamburg, Hamburg, Germany, respectively. Both consist of an upward-looking ADCP (Acoustic Doppler Current Profiler) mounted within a floatation body, additionally equipped with a SeaBird MicroCAT SBE 37 below the ADCP, providing temperature and salinity information. For the experiment in 2014/2015 DS20 had the same design and was positioned between DS1 and DS2. Further west, an ADCP and a MicroCAT were deployed as DS21 in a bottom mounted trawl proof frame. Mooring DS22 had an Aanderaa RCM8 and a MicroCAT and completed the array on the Greenlandic shelf. All of the ADCPs were "75-kHz Workhorse Long Rangers" from Teledyne RD Instruments. Further details about the mooring setup are provided in Jochumsen et al. (2017).

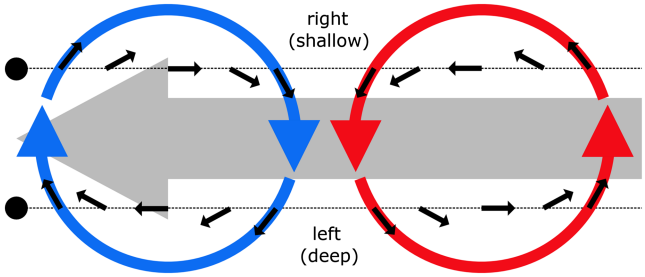

Figure 3. Scheme depicting a vector time series measured by moorings (black dots) during the passage of cyclonic (red) and anticyclonic (blue) eddies that are advected with the background flow (gray). Left (right) of the center of an eddy the vectors rotate counterclockwise (clockwise) over time, independent of the sense of rotation of the eddy. Adapted from Figure 15 of Darelius et al. (2011).

From the ADCPs we obtained vertical velocity profiles spanning 400 m with the first bin located 24 m above the bottom and a bin size of 16 m. The RCM performed single-point measurements at a height of 22 m above the bottom. The five moorings were separated by 5 to 10 km, thus spanning approximately 30 km from the deepest point of the passage toward the Greenlandic shelf (Figure 2). The temporal resolution of our data set is hourly and covers 300 days. MicroCAT data are considered to be representative of the homogeneous bottom layer, located within 50–100 m of the bottom (Rudels et al., 1999, 2005).

As a complementary data source we use a set of historical CTD profiles in the DS that were collected by the Institute of Oceanography of the University of Hamburg (e.g., Jochumsen, 2018). These CTD profiles provided the information depicted in Figure 2.

2.2. Data Quality Control and Postprocessing

The data were processed, quality controlled, and corrected as described in Jochumsen et al. (2017). The correction of the data took into account a low-velocity bias that affected the measurements of the Long Ranger ADCPs. The coordinate system was rotated such that the *v*-component is oriented along the mean flow direction and the *u*-component across the mean flow. Positive *v* is upstream (northeastward), and negative *v* is directed downstream (southwestward). Positive *u* is toward Iceland (southeastward), and negative *u* is directed toward Greenland (northwestward). As the flow follows topography, the components essentially correspond to along slope and across slope, respectively. In order to exclude tidal variations, the time series were detided using harmonic analysis (Pawlowicz et al., 2002). Tidal fluctuations were in the range of 0.2–0.3 m/s.

The maximum plume velocities were found on average within 100 m from the bottom (Jochumsen et al., 2017). We thus focus on this velocity level, except for DS22, where we use the measurements at 22 m above

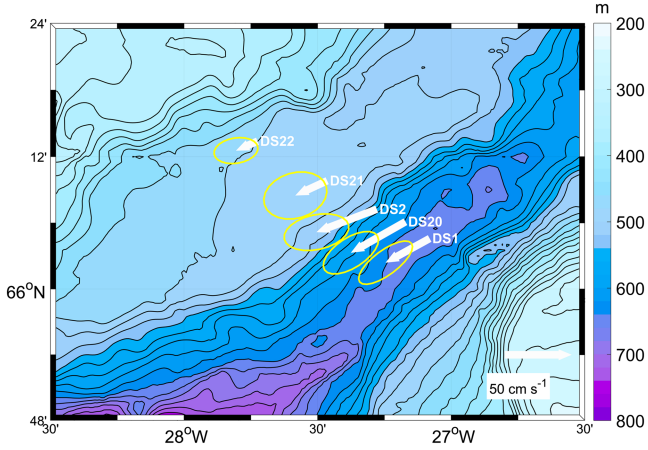

Figure 4. Mean velocity vectors 100 m above the bottom from 300 days of measurements. For DS22 the velocity is measured 22 m above the bottom. The yellow ellipses depict the standard deviation and are centered at the tip of each vector. The topography from the IBCAO v3 data set is shown in the background (Jakobsson et al., 2012).

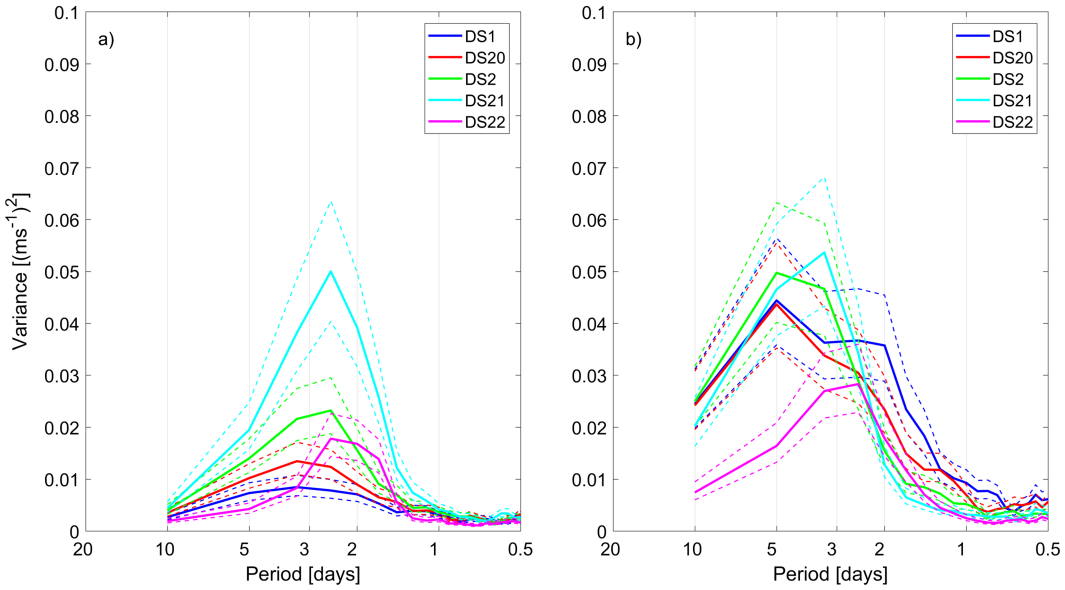

Figure 5. Variance preserving power spectra of (a) u (across-stream) and (b) v (along-stream) velocity components 100 m above the bottom for the DS mooring array in 2014/2015. For DS22 the velocity is obtained at 22 m above the bottom. Spectra are calculated using a Welch periodogram estimate for a 10-day window with 50% overlap to obtain a smoother result. The dotted lines indicate the respective 95% confidence intervals. DS = Denmark Strait.

the bottom, which is the height of the point measurement obtained by the current meter. For the location of DS22 we thus assume barotropic flow (as in Jochumsen et al., 2017). Barotropic structures were noted in velocity sections from the DS, showing horizontal scales of 30–50 km and varying in position (see figures in Girton et al., 2001; Jochumsen et al., 2015; Våge et al., 2011). However, this assumption may introduce errors as even this far toward Greenland the warm Atlantic layer can cover the upper water column and incline isopycnals (cf. Figure 2b).

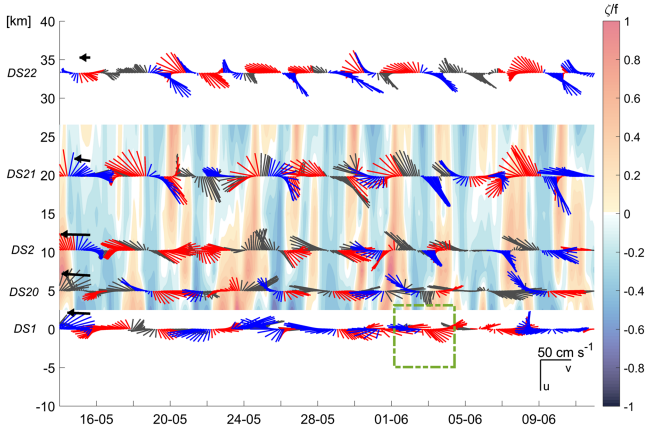

Figure 6. Low-pass filtered (13 hr) velocity anomaly vector time series for a 30-day period at 100 m above the bottom. The position of each mooring is indicated by their name and distance from the deepest point of the DS on the y axis. The bold black arrows on the left represent the mean velocity at each mooring. Vectors pointing to the left are in the downstream direction; vectors pointing up (down) are flow toward Greenland (Iceland). The reference scale is in the lower right corner. Background colors show the relative vorticity ζ normalized by f. Note that the contour plot gives an interpolated field, as the vorticity is only calculated in between mooring pairs. Cyclonic (anticyclonic) eddies are indicated by red (blue) vectors. Black vectors indicate that no eddy type could be identified. The green box indicates the example shown in Figure 7. DS = Denmark Strait.

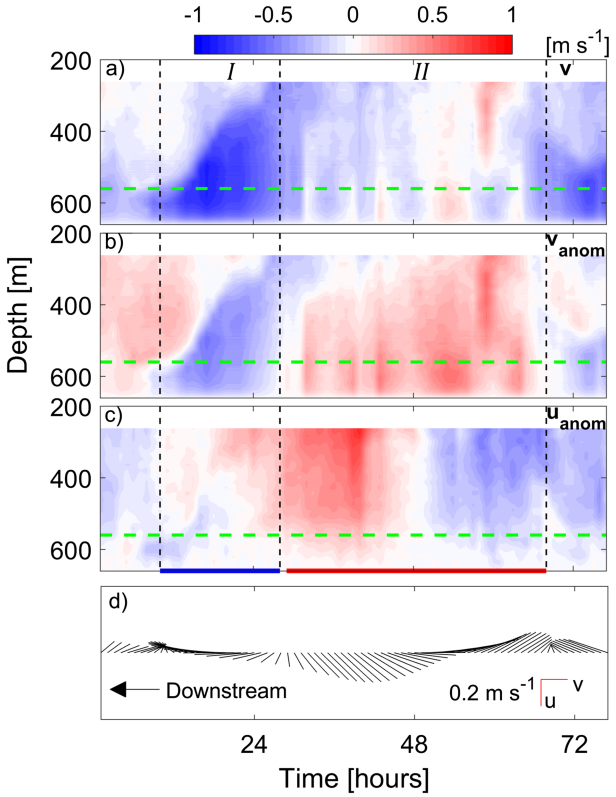

Figure 7. Hovmöller plots of (a) v and the anomalies (b) v' and (c) u' at DS1 during the passage of an anticyclone (I) followed by a cyclone (II). The time series of velocity anomaly vectors at 100 m above the bottom (green dotted line in a–c) is shown in (d). Eddy types are indicated by color at the bottom of panel (c), as in Figures 3 and 6. Negative v is directed downstream (southwestward), while positive u is directed southeastward.

2.3. Spectral Analysis

For spectral estimates of variance we applied Welch's periodogram method (Emery & Thomson, 2001). The time series were smoothed using a 10-day Hamming window. With a 50% overlap the spectra were averaged from 59 data segments.

2.4. Identification of Eddies

An eddy passing a current meter array can be identified in the recorded velocity time series by analyzing the changes of current directions. As illustrated in Figure 3 velocities measured to the left of the center of an eddy when looking downstream will rotate counterclockwise as the eddy passes the mooring. Similarly, a mooring on the right side of an eddy detects clockwise vector rotation, regardless of the eddy type passing by (see vectors along the dotted lines in Figure 3). The sense of eddy rotation can nevertheless be determined by the orientation of the velocity vectors at the beginning of the rotation sequence: For an anticyclone the starting vector is positive (upward in Figure 3) and negative for a cyclone (pointing downward in Figure 3). By combining this information, passing eddies can be detected from a vector time series, as shown in Foldvik et al. (1988) and Darelius et al. (2011).

When the center of an eddy passes directly over a mooring, the measured vector rotation will be 180°. However, this only rarely occurs in practice. Most often a mooring will capture the eddy off center and the resulting rotation in the vector time series will be less than 180°(see Figure 3 and Figure 15 in Darelius et al., 2011). The total vector rotation decreases with distance from the eddy center. A threshold value <180° must be found, which allows for eddies not fully captured by the measurement to be detected, but excludes fluctuation due to other features. We use 45° here, which is a compromise of the two goals. Furthermore, we introduced a time threshold, which requires eddy events at the moorings to last at least 13 hr, during which the change of rotation must be persistent (i.e., always following the same sense of rotation, either clockwise or anticlockwise).

Table 1
Statistics of Eddy Types—Cyclonic (Cycl.) or Anticyclonic (Anticycl.) Rotation—Derived From the Band-Pass Filtered (13-hr Low Pass) Time Series

Mooring	DS1	DS20	DS2	DS21	DS22
Eddy Type	anticycl.(cycl.)	anticycl. (cycl.)	anticycl.(cycl.)	anticycl. (cycl.)	anticycl.(cycl.)
Number	75 (56)	71 (80)	53 (89)	75 (94)	85 (85)
Duration (days)	0.9 (1.0)	0.9 (0.9)	1.0 (0.9)	1.0 (1.0)	1.0 (1.0)
v_{adv} (m/s)	0.35 (0.40)	0.45 (0.48)	0.48 (0.48)	0.26 (0.26)	0.19 (0.16)
Diameter (km)	28 (36)	35 (37)	42 (39)	23 (22)	16 (14)
EKE (cm^2/s^2)	473 (389)	424 (403)	436 (477)	428 (479)	262 (236)
T_{bot} (°C)	0.04(−0.03)	0.04 (−0.02)	0.05(−0.05)	0.02 (0.00)	0.03 (−0.02)
h (m)	−12 (30)	−11 (16)	−4 (0)	−16 (4)	8 (−6)

Note. Statistics considered were number of observed eddies, the time it took them to pass the mooring array (Duration), the velocity at which the eddy is advected across the mooring array (v_{adv}), eddy diameter, eddy kinetic energy (EKE) obtained from velocity anomalies, near-bottom water temperature measured at the mooring (T_{bot}), and the plume thickness (h) as an offset from the average plume height. DS = Denmark Strait; EKE = eddy kinetic energy.

The analysis described above was applied to our mooring time series after detiding. In addition, to reduce short-term fluctuations that interrupt the vector rotation and thus disturb the eddy detection algorithm, a fourth-order Butterworth filter with a 13-hr cutoff was applied. From the resulting time series of velocity anomalies, events lasting at least 13 hr (i.e., consistent clockwise or anticlockwise rotation) were identified. The orientation of the velocity vector at the beginning of each event was used to assign an eddy type. As a result, each velocity measurement was assigned an eddy type (cyclone-east, cyclone-west, anticyclone-east, and anticyclone-west) or a no-eddy flag. This approach allowed eddies to be identified from velocity anomalies alone, without any assumptions about their structure or fits to specific shapes.

All vector stick plots in the following show the detided, 13-hr low-pass filtered time series of velocity anomalies. Figures of velocity components present the unfiltered but detided velocity anomaly data.

Once we identified eddy types in the time series, we calculated for each eddy type the eddy kinetic energy as $EKE = \overline{\frac{1}{2}(u'^2 + v'^2)}$, where the overbar denotes the time-mean over all eddies of a type in the total time series and u' and v' are the velocity anomalies of individual eddies (i.e., after removing their mean).

An alternative approach to identify eddies is to calculate the relative vorticity $\zeta = \frac{dv}{dx} - \frac{du}{dy}$, which is positive (negative) for cyclones (anticyclones). As the mooring array is set up in a line perpendicular to the mean flow direction the cross-stream gradient could be calculated directly. For the along-stream gradient we use advective time derivatives, assuming that du is advected with the mean flow as an eddy property. In the following the "eddy core" is defined as the region where the derivative of the cross-stream velocity remains relatively constant. It is therefore bounded by a change in the sign of the derivative of the cross-stream velocity, that is, when the velocity stops increasing (decreasing) and begins to decrease (increase).

3. Results

3.1. Velocity Field

For all five moorings, the time-mean velocity vectors are generally orientated along the topography at 245 ± 4° relative to true north (Figure 4). The highest mean velocities are found at the central mooring sites (DS20/DS2: 0.47/0.48 m/s), located near the deepest part of the strait. The standard deviation is of the same order at all sites (≈0.3 m/s), except at DS22 (≈0.2 m/s). The standard deviation ellipses show that the major axis is oriented along the topography. Ellipses at DS2 are directed about 20° cross slope according to the mapped contour lines determined from the IBCAO data set (Jakobsson et al., 2012). The horizontal velocity shear implies positive relative vorticity (cyclonic rotation) to the east and negative relative vorticity to the west (anticyclonic rotation) of DS2.

Variations in the cross-stream velocity u can be attributed to a lateral distortion of the flow, while fluctuations in the along-stream component v indicate a strengthening or weakening of the mean flow. Both types of variation can be caused by the passage of eddies, the lateral movement of the NIIC front, or the occurrence

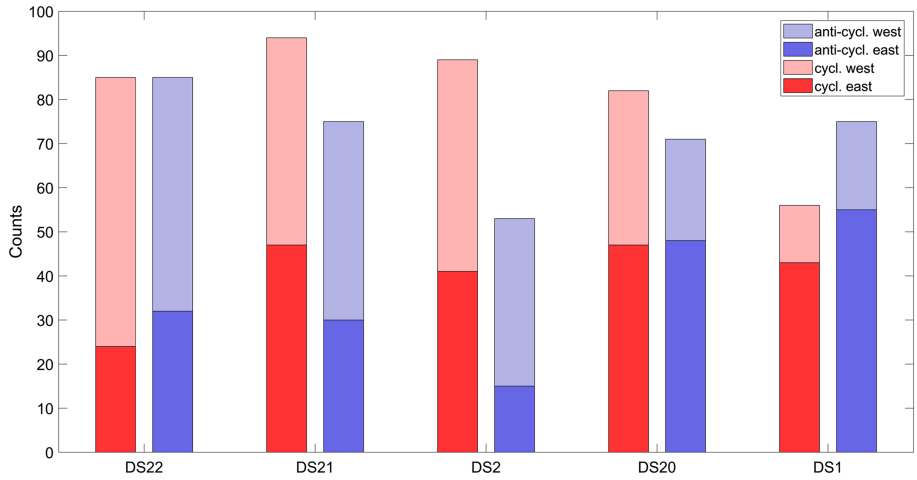

Figure 8. Histogram of the occurrence of anticyclones (blue) and cyclones (red) at each mooring site. Dark (light) colors indicate that the location of the measurement (mooring position) was on the eastern (western) side relative to the eddy center.

of boluses and pulses (von Appen et al., 2017). The variance preserving power spectra of the detided u and v velocity components are presented in Figure 5.

The variance in u increases from the deepest point of the passage (DS1) toward the Greenland shelf, with the highest variance at DS21, whose peak spans periods of about 2 to 3 days (Figure 5a). The amplitude of the variance in v is of the same range for all moorings (Figure 5b).The maxima in the spectra shift from 5 to about 3 days as we move from east (DS1) to west (DS21). At mooring DS1, which is closest to the NICC front, pronounced energy is also found at a period of about 2 days. With the exception of DS21, the variability at the mooring sites is dominated by the along-stream component, following the topography, indicating fluctuations in the overflow strength.

3.2. Eddy Properties

Figure 6 presents the results of the eddy identification process, as explained in section 2.4, for a month of data at all five moorings. In general, the vectors show the successive passage of cyclones and anticyclones. They appear in a variety of sizes and strengths, with regard to the velocity magnitude.

The vorticity also shows alternating patterns, indicating that eddies of different types are passing the array. Both methods match in about 65% of cases. When the two methods agree, the core of an eddy has likely been found, that is, red (blue) sticks and positive (negative) vorticity identify cyclonic (anticyclonic) vortices. The vorticity changes sign every 0.8 to 1.2 days. The sign change can occur when an eddy core is entering or leaving the mooring location and thus gives a hint on the duration and size of a passing eddy. Eddy diameters were obtained from the duration of an eddy event (eddy persistence) and the background velocity, taken as the mean of the unfiltered, detided time series for each event. As a rough estimate the diameters are on the order of 35 km, assuming that an eddy is translating across the array within 24 hr and is advected with a mean velocity of about 0.4 m/s. Eddy diameters obtained from this procedure do not prescribe a circular shape but give the eddy dimension in along-stream direction. If an eddy was captured off center, the estimated diameter is biased to smaller values.

An example of two identified eddies, an anticyclone (I) followed by a cyclone (II), is shown in more detail in Figure 7 and can be compared to the identification scheme in Figure 3. In this example both eddies are registered at mooring DS1 on their eastern flank. During the presence of the anticyclone (period marked as I in Figure 7) the velocity anomaly vectors rotate counterclockwise (panel d), from a downstream to an across-stream (toward Iceland) direction. The total downstream flow increases (panel a). When the cyclone arrives at the mooring, the v' and u' components increase (panels b and c), reducing the total downstream flow and eventually reversing it. The transit of the anticyclone and cyclone takes 18 and 39 hr, respectively. The signal of the anticyclone appears to be baroclinic (first detected at depth then apparent throughout the water column), while the signature of the cyclone is rather barotropic.

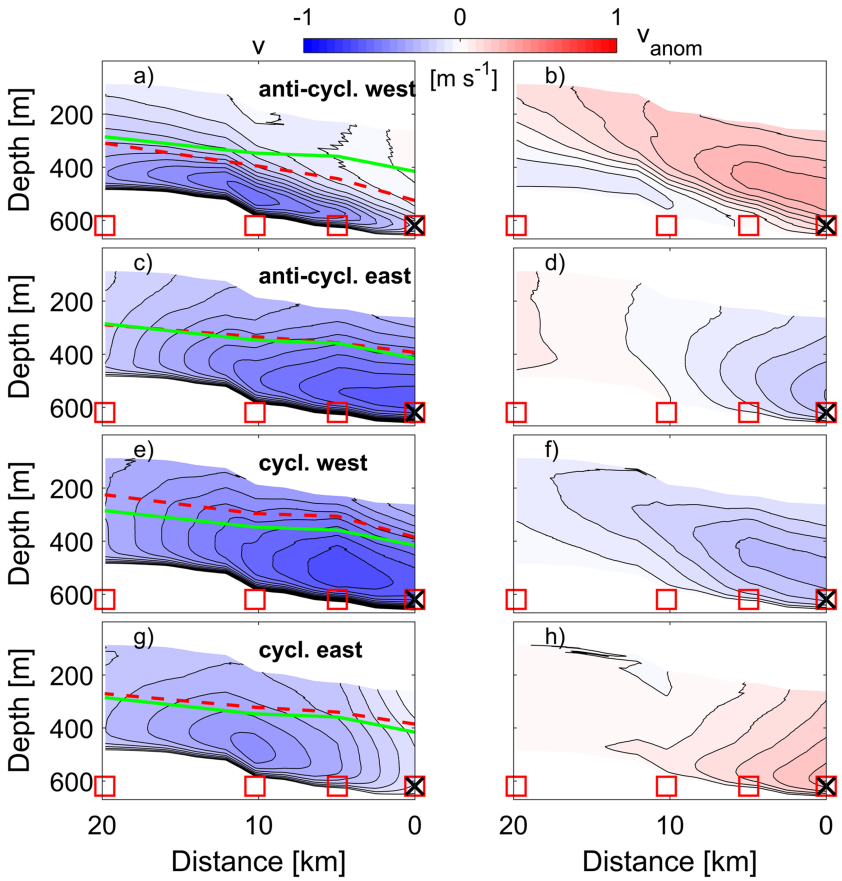

Figure 9. Composites of downstream velocity v (left column) and velocity anomalies v' (right column) for different eddy cases registered at (Denmark Strait) DS1: western flank of anticyclone (a, b), eastern flank of anticyclone (c, d), western flank of cyclone (e, f), and eastern flank of cyclone (g, h). The red squares denote the mooring positions with DS1 as the easternmost mooring (black cross; DS22 is not included). The green line denotes the average plume thickness derived from the depth of maximum shear; the red dashed line denotes the average thickness for the particular eddy case.

Applying the vector method to the full time series of all moorings, we can determine average eddy property statistics, as summarized in Table 1. The number of eddy types and the location relative to the eddy center for each mooring site is shown in Figure 8. Moorings west (east) of DS20 are located more frequently on the western (eastern) side of both cyclones and anticyclones. West of DS1 cyclones outnumber anticyclones by about 68% (53 anticyclones and 89 cyclones at DS21). At DS22 the distribution of eddy types is even. Thus, we conclude that the center of an eddy is most likely to be found near DS20 or between DS20 and DS2, which corresponds to the highest mean velocities and the average position of the plume core. Both anticyclones and cyclones have periods of about 3 to 6 days. Dividing the total number of identified eddies by the length of the time series (300 days) indicates that approximately every 2 days, an eddy, anticyclone, or cyclone is registered. The time it takes an eddy to pass through the mooring array is about 1 day, which agrees with the change of vorticity after about 1 day, and does not vary considerably with eddy type.

By combining the time it takes for an eddy to cross the sill with the advective velocities, the average eddy diameter ranges between 14 and 42 km, depending on the mooring (Table 1). East of DS2, cyclones are slightly larger than anticyclones. The largest diameters are found at DS20 and DS2, which again indicates that the eddy centers pass near these moorings and that the full eddy diameters exceed 35 km (Table 1). The thickness of the plume h is derived from the maximum in vertical velocity shear (Jochumsen et al., 2017). On average the plume is slightly thinner (-7 ± 10 m) during the passage of anticyclones and thicker (9 ± 15 m) during the passage of cyclones. The difference in thickness is small, that is, less than 15 m on average, which is smaller than the bin size of the ADCPs, indicating that these differences may not be statistically significant. Only at DS1 does the thickness of the plume increase considerably when a cyclone is passing.

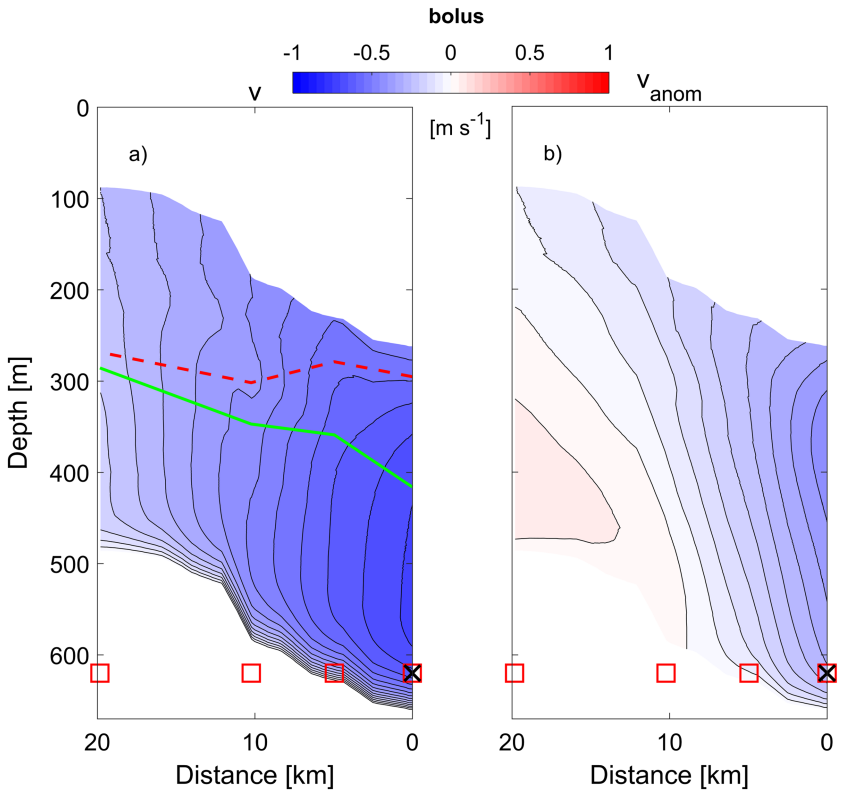

Figure 10. Composites of (a) downstream velocity v and (b) velocity anomalies v' for boluses registered at DS1. The green line denotes the average plume thickness derived from the depth of maximum shear; the red dashed line denotes the average thickness for boluses.

The highest EKE (>470 cm^2/s^2) is found for cyclones at DS2 and DS21 and anticyclones at DS1. The largest difference (85 cm^2/s) between eddy types is seen at DS1, where anticyclones are more energetic than cyclones. At DS2 and DS21 EKE values are larger for cyclones. The difference in EKE between eddy types is smallest at DS20 and DS22. Note that the lower average value at DS22 is likely caused by the measurements being taken close to the bottom where velocity variations are smaller.

During the passage of cyclones bottom temperatures are lower than the mean (−0.03 °C) and anticyclones can be connected to positive temperature anomalies (0.04 °C). However, the temperature difference is below O(0.1 °C), which is relatively small compared to overall variability of bottom temperature (the standard deviation of temperature at DS1 is 0.6 °C).

Composites of the downstream velocity and its anomaly were calculated for the full mooring array, separately for the four eddy types (i.e., rotation and location in the eddy) identified at DS1 (Figure 9). When DS1 captures the western side of an anticyclone, the plume tends to be 110 m thinner at DS1; there is a northeastward velocity anomaly, and the plume core identified by the maximum southwestward velocity is located near DS2 (Figures 9a and 9b). If the eastern side of an anticyclone is captured by DS1, the southwestward flow increases and the plume core is located at DS1 or further east, on the Icelandic side of the strait. The plume thickness increases slightly (by 22 m at DS1; Figures 9c and 9d) and the velocity anomaly is mainly barotropic. A passing cyclone that is captured on its western flank by DS1 causes an increase of southwestward flow at DS1, a thicker plume (+30 m at DS1), and the plume core shifts its location to DS20 (Figures 9e and 9f). The pattern of the velocity anomaly resembles the first case (western side, anticyclone) but with opposite sign. When the eastern flank of a cyclone is captured, the southwestward flow is reduced, the plume is slightly thicker (+30 m at DS1), and the core is located near DS2 (Figures 9g and 9h). The velocity anomaly is again mainly barotropic.

To test the robustness of this result, we recalculated the composites in Figure 9 but only for cases where the same eddy type was detected simultaneously at DS1 and the neighboring DS20. This criterion holds in one

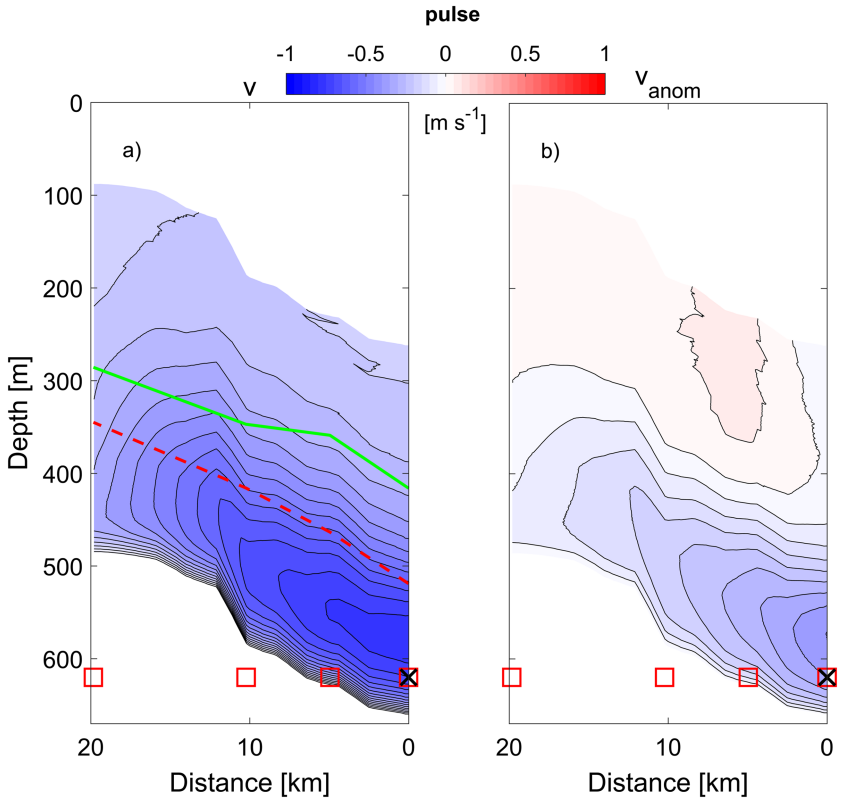

Figure 11. Composites of (a) downstream velocity v and (b) velocity anomalies v' for pulses registered at DS1. The green line denotes the average plume thickness derived from the depth of maximum shear; the red dashed line denotes the average thickness for boluses.

third of the detected eddy events at these locations. The resulting composites (not shown) have generally the same patterns but with a slight increase in velocity magnitude and a shift toward the west.

3.3. Boluses and Pulses

Another important set of mesoscale features found at the DS sill are boluses and pulses (Almansi et al., 2017; Mastropole et al., 2017; von Appen et al., 2017). We use our data set to identify such phenomena and relate them to the occurrence of eddies. In order to do so, we first define criteria to identify boluses and pulses. For a bolus, the downstream velocity must be strong (>75th percentile) and the plume thick (>75th percentile). For a pulse, the downstream velocity must be strong (> 75th percentile) as well but the plume thin (< 25th percentile). We then create composites of the velocity field for times these criteria match. A bolus registered at DS1 is associated with a barotropic increase of downstream flow (Figure 10). For a pulse we find a baroclinic structure with an anomaly of upstream flow in the upper layer and downstream flow

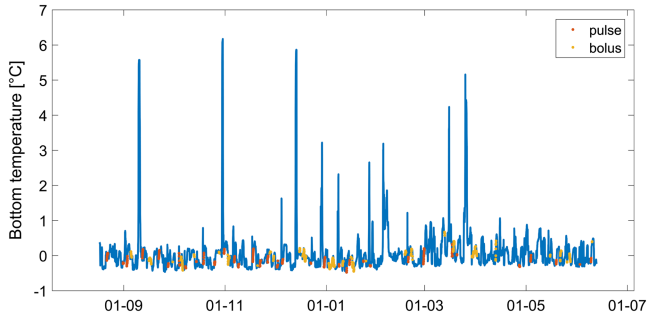

Figure 12. Time series of bottom temperature at DS1 during the mooring period 2014/2015. Times where pulses (red) and boluses (yellow) were identified are highlighted.

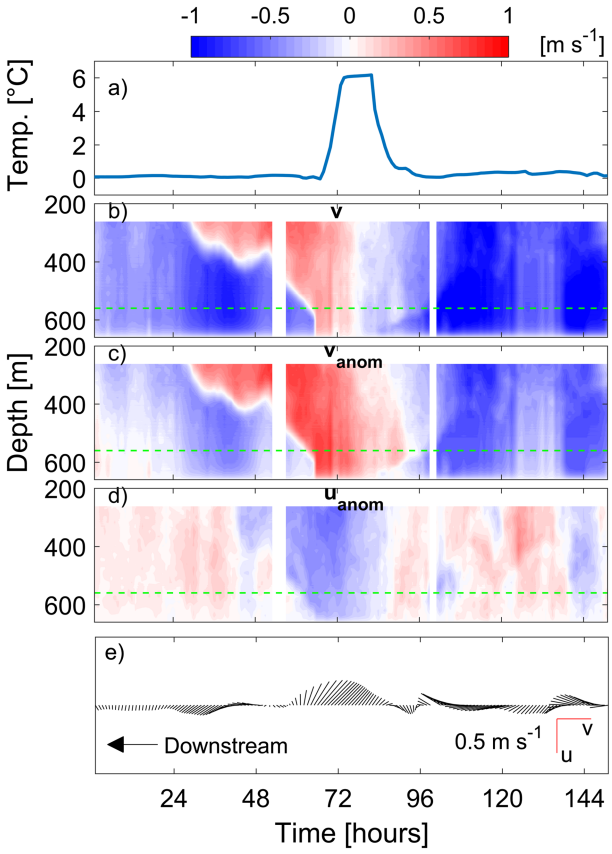

Figure 13. Time series of (a) bottom temperature at DS1 during a warm event and Hovmöller plots of (b) downstream velocity v and the anomalies (c) v' and (d) u' at DS1. The time series of velocity anomaly vectors at 100 m above the bottom (green dotted line in b–d) is shown in (e). The time axis starts on 27 October 2014, 6:00.

in the bottom layer (Figure 11). About 60% of all detected boluses and pulses do not coincide with eddies identified with the methods described earlier. However, there are occasions when the passage of a pulse (42%) or a bolus (28%) corresponds to the transit of the eastern flank of an anticyclone (Figure 9c). This agrees with the counterclockwise vector rotation in Figure 9 of von Appen et al. (2017).

3.4. Meandering of the NIIC

Bottom temperatures measured at DS1 show strong fluctuations with very warm events that exceed 2 and even 4 °C (Figure 12). This signal is likely caused by a westward shift of the NIIC front and can be observed at all moorings (not shown). As an example, Figure 13 shows the evolution of the warmest event observed during the mooring period. At first, the flow is weak and approximately southward throughout the water column. After a day the velocities increase and, in the upper layer, rapidly rotate toward the north. After 72 hr, northward flow occupies the whole water column and the near-bottom temperature has increased to 6 °C. This situation persists for about 10 hr and then returns to a weak southward flow. Overall, temperatures exceeded 4 °C at DS1 on five separate occasions. With one exception (western flank of an anticyclone) these warm events do not correspond to observed eddies. In addition, no obvious relation to a bolus or pulse is evident (cf. Figure 12).

4. Discussion and Conclusion

In this study, data from five moorings were used to analyze the mesoscale variability of the overflow at the Denmark Strait sill on time scales of 1 to 10 days. Trains of eddies were identified, alternating cyclones and anticyclones, by distinguishing unique patterns in anomalies of the velocity field. In addition, boluses and pulses were detected at the deepest part of the strait, and their presence was occasionally connected to a

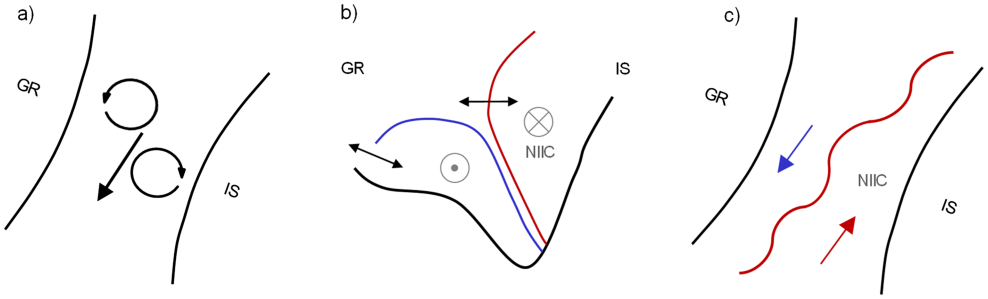

Figure 14. The variability of the flow through the Denmark Strait between the Greenlandic (GR) and Icelandic shelves (IS) is influenced by (a) the passage of mesoscale vortices (eddies), (b) the lateral movement of the dense plume (blue) up and down the slope of the Greenlandic shelf and the movement of the NIIC front (red), and (c) the instability and meandering of the NIIC front (red) .

passing anticyclone. These features are likely linked to frontal instabilities of the NIIC, which also cause temperature fluctuations at the mooring array of more than 4 °C. The drivers of mesoscale variability identified in this study are summarized in Figure 14 and discussed in more detail below.

4.1. Cyclonic and Anticyclonic Eddies

The analysis of the vector rotation and vorticity shows alternating patterns and suggests that trains of cyclones and anticyclones are propagating across the sill. The eddies have periods of about 3 to 6 days and diameters on the order of 30 to 40 km. Previous studies north and south of the sill have found similar sizes and frequencies (e.g., Bruce, 1995; Foldvik et al., 1988; Harden et al., 2016; Krauss, 1996; Lundrigan & Demirov, 2019), as well as the presence of trains of eddies (e.g., Jungclaus et al., 2001). However, downstream of the DS sill, cyclones dominate the deep overflow and anticyclones are found on the shallower side of the Greenland slope, supposedly caused by vortex stretching and squeezing (Krauss & Käse, 1998; Shi et al., 2001). This discrepancy suggests that the eddies observed at the sill are formed by different mechanisms than those found downstream. This is perhaps due to the more gradual topography at the saddle point or conditions upstream of the sill not captured by this analysis. A possible source of eddies is the meandering of the NIIC front (see below), which could also explain the occurrence of anticyclones in the deep part of the strait: anticyclones formed from the NIIC front would tend to occupy the deep and western side of the sill, while the formation of cyclones would be hindered by the limitation of space on the eastern side (the steep Icelandic shelf break) .

The estimated EKE differs between the two eddy types. Maximum EKE values are about 480 cm^2/s^2 and correspond to anticyclones at the eastern moorings (DS1 and DS20) and cyclones at the western moorings (DS2 and DS21). Our EKE estimates are about 3 times larger than average near-surface EKE at the Kögur section (200 km north of the sill) presented in Håvik et al. (2017). They also exceed estimates south of the sill (array A presented in Voet & Quadfasel, 2010).

4.2. Boluses and Pulses

Previous studies linked the development of cyclonic and anticyclonic eddies with the formation and propagation of boluses of dense water south of the sill (Jungclaus et al., 2001; Shi et al., 2001). However, in a more recent and extensive study von Appen et al. (2017) conclude that neither boluses nor pulses are linked with eddies. Our results form a link between these two views, as we have occasionally connected boluses and pulses to an anticyclone passing DS1. Only this eddy case offers the conditions where a bolus or pulse can accompany an eddy. None of the other eddy cases provide sufficiently strong negative velocity anomalies at DS1, which distinguish both boluses and pulses from the mean flow (see Figure 9). However, when an anticyclone passes the strait with its center close to the Greenland slope, that is, mooring DS1 is on the eastern flank of the eddy, the velocity field is altered to strong downstream flow (Figures 9c and 9d). The overflow thickness varies around its mean for this eddy case, allowing for both boluses and pulses: Strong positive anomalies in overflow thickness indicate a bolus, while strong negative anomalies correspond to a pulse.

4.3. Meandering of the NIIC

The bottom temperatures vary on hourly to daily scales, but this variability is distorted by sporadic extreme warming events that exceed 4 °C. Occasionally, the warm water peaks are even registered at the westernmost mooring DS22 (not shown). It is likely that the warm water originates in the vicinity of the sill,

where bottom temperatures in the northward flow are within the observed range (e.g., see Figure 1 in Jochumsen et al., 2015). Further north of the sill, similarly high temperatures are not found below approximately 350 m (Jónsson & Valdimarsson, 2004, 2012; Smith, 1976). In agreement with recent findings by Spall et al. (2019), we conclude that the warming events are caused by the meandering of the NIIC front, as the westward movement of the cold overflow plume allows the warm water of Atlantic origin to temporarily occupy the array (Jochumsen et al., 2012). The shift of the NIIC front is connected to the occurrence of pulses (Spall et al., 2019; von Appen et al., 2017) and anticyclonic patterns in the velocity field.

4.4. Sensitivity of the Eddy Identification Method

The eddy identification method includes thresholds that, depending on their choice, affect the results, that is, eddy statistics (Table 1). To evaluate the sensitivity of the results to the identification method, we reran the identification algorithm with various settings. The most important threshold is the minimum rotation angle of the low-pass filtered velocity vectors (cf. section 2.4). An adjustment of this threshold results in a different number of eddies detected. By reducing the angle, more eddies are identified, that is, 5% to 10% more for an angle of 30°. When increasing the threshold, less eddies are identified, that is, 20% to 50% less for an angle of 90°and 50% to 70% less for an angle of 120°. While the duration and diameter do not change significantly, at a larger threshold of 90° and 120°, the ratio between the number of anticyclones and cyclones changes slightly and the EKE reduces by 20% and 30% on average, respectively. Therefore, a rotation angle threshold below 45 results in little change, while a higher threshold misses many eddies that only pass through a portion of the array but are still relevant to the study.

4.5. Conclusion and Outlook

Our observational analysis at the DS sill emphasizes the importance of eddies for short-term flow variability. Altogether, eddies, boluses, and pulses and the meandering of the NIIC front form a wealth of mesoscale features detected at this location. We cannot determine from our data if these features are produced by as many processes or simply correspond to phases of the same instability process. Resolving the forcing and effect of these features requires high-resolution observational data or model configurations. As a result, estimates of the overflow strength are potentially susceptible to aliasing, that is, when a mooring is capturing a predominant side of the eddies, the mean velocity at the mooring location can be biased.

Open questions remain regarding the formation process of the sill eddies, as vortex stretching and squeezing cannot be accountable at this location. High-resolution modeling studies could provide answers, although topographic features may very well play a role, which are a challenge to capture realistically in models. The lifetime, pathway, and dissipation of the sill eddies will be addressed in further studies, eventually linking the features to downstream overflow modification (North et al., 2018) and eddy features off Greenland (von Appen et al., 2014).

Acknowledgments

We thank the crew of the German research vessel Poseidon and mooring technicians for their highly appreciated support during deployment and recovery of the instruments. We thank Bob Pickart for helpful discussions. We appreciate the valuable comments and suggestions of the anonymous reviewers. Financial support was given by the Co-Operative Project RACE II "Regional Atlantic Circulation and Global Change" funded by the German Federal Ministry for Education and Research (BMBF), Förderkennzeichen 03F0729B and the project "Energy transfers in gravity plumes" of the Collaborative Research Centre TRR 181 "Energy Transfer in Atmosphere and Ocean" funded by the German Research Foundation. The velocity and bottom temperature records from the array 2014/2015 used in this study are available on the Zenodo repository (DOI: 10.5281/zenodo.2658886). CTD data from RV Poseidon cruise POS 471 and RV Maria S. Merian MSM21/b are available on the Pangaea webpage (Jochumsen, 2018; Krahmann, 2016).

References

Almansi, M., Haine, T. W. N., Pickart, R. S., Magaldi, M. G., Gelderloos, R., & Mastropole, D. (2017). High-frequency variability in the circulation and hydrography of the Denmark Strait overflow from a high-resolution numerical model. *Journal of Physical Oceanography*, *47*(12), 2999–3013. https://doi.org/10.1175/JPO-D-17-0129.1

Bruce, J. (1995). Eddies southwest of the Denmark Strait. *Deep Sea Research Part I: Oceanographic Research Papers*, *42*(1), 13–29. https://doi.org/10.1016/0967-0637(94)00040-Y

Darelius, E., Fer, I., & Quadfasel, D. (2011). Faroe Bank Channel Overflow: Mesoscale Variability. *Journal of Physical Oceanography*, *41*(11), 2137–2154. https://doi.org/10.1175/JPO-D-11-035.1

Emery, W. J., & Thomson, R. E. (2001). *Data Analysis Methods in Physical Oceanography* (2nd ed.). Boulder: Elsevier B.V.

Fischer, J., Karstensen, J., Zantopp, R., Visbeck, M., Biastoch, A., Behrens, E., et al. (2015). Intra-seasonal variability of the DWBC in the western subpolar North Atlantic. *Progress in Oceanography*, *132*, 233–249. https://doi.org/10.1016/j.pocean.2014.04.002

Foldvik, A., Aagaard, K., & Toerresen, T. (1988). On the velocity field of the East Greenland Current. *Deep Sea Research Part A. Oceanographic Research Papers*, *35*(8), 1335–1354. https://doi.org/10.1016/0198-0149(88)90086-6

Fristedt, T., Hietala, R., & Lundberg, P. (1999). Stability properties of a barotropic surface-water jet observed in the Denmark Strait. *Tellus A*, *51*(5), 979–989. https://doi.org/10.1034/j.1600-0870.1999.00030.x

Girton, J., Sanford, T., & Käse, R. (2001). Synoptic sections of the Denmark Strait Overflow. *Geophysical Research Letters*, *28*(8), 1619–1622. https://doi.org/10.1029/2000GL011970

Håvik, L., Våge, K., Pickart, R. S., Harden, B., von Appen, W.-J., Jónsson, S., & Østerhus, S. (2017). Structure and variability of the Shelfbreak East Greenland Current north of Denmark Strait. *Journal of Physical Oceanography*, *47*(10), 2631–2646. https://doi.org/10.1175/JPO-D-17-0062.1

Hansen, B., Østerhus, S., Turrell, W. R., Jónsson, S., Valdimarsson, H., Hátún, H., & Olsen, S. M. (2008). The Inflow of Atlantic water, Heat, and Salt to the Nordic Seas across the Greenland-Scotland Ridge. In R. R. Dickson, J. Meincke, & P. Rhines (Eds.), *Arctic-subarctic ocean fluxes: Defining the role of the northern seas in climate* (pp. 15–43). Dordrecht: Springer Netherlands.

Harden, B., Pickart, R. S., Valdimarsson, H., Våge, K., de Steur, L., Richards, C., et al. (2016). Upstream sources of the Denmark Strait Overflow: Observations from a high-resolution mooring array. *Deep Sea Research I*, *112*, 94–112. https://doi.org/10.1016/j.dsr.2016.02.007

Jakobsson, M., Mayer, L., Coakley, B., Dowdeswell, J. A., Forbes, S., Fridman, B., et al. (2012). The International Bathymetric Chart of the Arctic Ocean (IBCAO) Version 3.0. *Geophysical Research Letters*, *39*, L12609. https://doi.org/10.1029/2012GL052219

Jochumsen, K. (2018). Physical oceanography during POSEIDON cruise POS471/2 and POS471/3. [data set]. PANGAEAhttps://doi.org/10.1594/PANGAEA.890821

Jochumsen, K., Köllner, M., Quadfasel, D., Dye, S., Rudels, B., & Valdimarsson, H. (2015). On the origin and propagation of Denmark Strait over flow water anomalies in the Irminger Basin. *Journal of Geophysical Research: Oceans*, *120*, 1841–1855. https://doi.org/10.1002/2014JC010397

Jochumsen, K., Moritz, M., Nunes, N., Quadfasel, D., Larsen, K. M. H., Hansen, B., et al. (2017). Revised transport estimates of the Denmark Strait overflow. *Journal of Geophysical Research: Oceans*, *122*, 3434–3450. https://doi.org/10.1002/2017JC012803

Jochumsen, K., Quadfasel, D., Valdimarsson, H., & Jónsson, S. (2012). Variability of the Denmark Strait overflow: Moored time series from 1996-2011. *Journal of Geophysical Research*, *117*, C12003. https://doi.org/10.1029/2012JC008244

Jónsson, S., & Valdimarsson, H. (2004). A new path for the Denmark Strait overflow water from the Iceland Sea to Denmark Strait. *Geophysical Research Letters*, *31*, L03305. https://doi.org/10.1029/2003GL019214

Jónsson, S., & Valdimarsson, H. (2012). Water mass transport variability to the North Icelandic shelf, 1994-2010. *ICES Journal of Marine Science*, *69*(5), 809. https://doi.org/10.1093/icesjms/fss024

Jungclaus, J. H., Hauser, J., & Käse, R. H. (2001). Cyclogenesis in the Denmark Strait overflow plume. *Journal of Physical Oceanography*, *31*(11), 3214–3229. https://doi.org/10.1175/1520-0485(2001)031\$<\$3214:CITDSO\$>\$2.0.CO;2

Käse, R. H., & Oschlies, A. (2000). Flow through Denmark Strait. *Journal of Geophysical Research*, *105*(C12), 28,527–28,546. https://doi.org/10.1029/2000JC900111

Krahmann, G. (2016). Physical oceanography during Maria S. Merian cruise MSM21/1b. [data set]. PANGAEA https://doi.org/10.1594/PANGAEA.859599, .

Krauss, W. (1996). A note on over flow eddies. *Deep Sea Research Part I: Oceanographic Research Papers*, *43*(10), 1661–1667. https://doi.org/10.1016/S0967-0637(96)00073-8

Krauss, W., & Käse, R. H. (1998). Eddy formation in the Denmark Strait overflow. *Journal of Geophysical Research*, *103*(C8), 15,525–15,538. https://doi.org/10.1029/98JC00785

Latarius, K., & Quadfasel, D. (2016). Water mass transformation in the deep basins of the nordic seas: Analyses of heat and freshwater budgets. *Deep Sea Research*, *114*, 23–42. https://doi.org/10.1016/j.dsr.2016.04.012

Lundrigan, S., & Demirov, E. (2019). Mean and eddy-driven heat advection in the ocean region adjacent to the Greenland-Scotland Ridge derived from satellite altimetry. *Journal of Geophysical Research: Oceans*, *124*, 2239–2260. https://doi.org/10.1029/2018JC014854

Macrander, A., Käse, R. H., Send, U., Valdimarsson, H., & Jónsson, S. (2007). Spatial and temporal structure of the Denmark Strait overflow revealed by acoustic observations. *Ocean Dynamics*, *57*(2), 75–89. https://doi.org/10.1007/s10236-007-0101-x

Mastropole, D., Pickart, R. S., Valdimarsson, H., Våge, K., Jochumsen, K., & Girton, J. (2017). On the hydrography of Denmark Strait. *Journal of Geophysical Research: Oceans*, *122*, 306–321. https://doi.org/10.1002/2016JC012007

Mauritzen, C. (1996). Production of dense over flow waters feeding the North Atlantic across the Greenland-Scotland Ridge. Part 1: Evidence for a revised circulation scheme. *Deep Sea Research Part I: Oceanographic Research Papers*, *43*(6), 769–806. https://doi.org/10.1016/0967-0637(96)00037-4

North, R. P., Jochumsen, K., & Moritz, M. (2018). Entrainment and energy transfer variability along the descending path of the Denmark Strait overflow plume. *Journal of Geophysical Research: Oceans*, *123*, 2795–2807. https://doi.org/10.1002/2018JC013821

Nurser, A. J. G., & Bacon, S. (2014). The Rossby radius in the Arctic Ocean. *Ocean Science*, *10*, 967–975. https://doi.org/10.5194/os-10-967-2014

Pawlowicz, R., Beardsley, B., & Lentz, S. (2002). Classical tidal harmonic analysis including error estimates in MATLAB using T_TIDE. *Computers and Geosciences*, *28*, 929–937.

Pickart, R. S., & Watts, D. R. (1990). Deep western boundary current variability at Cape Hatteras. *Journal of Marine Research*, *48*(4), 765–791. https://doi.org/10.1357/002224090784988674

Quadfasel, D., & Käse, R. (2007). Present-Day Manifestation of the Nordic Seas Overflows. In A. Schmittner (Ed.), *Ocean Circulation: Mechanisms and Impacts*, Geophysical Monograph Series (Vol. 173, pp. 75–90), . Washington, DC: American Geophysical Union. https://doi.org/10.1029/173GM07

Rudels, B., Björk, G., Nilsson, J., Winsor, P., Lake, I., & Nohr, C. (2005). The interaction between waters from the Arctic Ocean and the Nordic Seas north of Fram Strait and along the East Greenland Current: Results from the Arctic Ocean-02 Oden expedition. *Journal of Marine Systems*, *55*, 1–30. https://doi.org/10.1016/j.jmarsys.2004.06.008

Rudels, B., Eriksson, P., Grönvall, H., Hietala, R., & Launiainen, J. (1999). Hydrographic observations in Denmark Strait in fall 1997, and their implications for the entrainment into the overflow plume. *Geophysical Research Letters*, *26*(9), 1325–1328. https://doi.org/10.1029/1999GL900212

Shi, X. B., Roed, L. P., & Hackett, B. (2001). Variability of the Denmark Strait overflow: A numerical study. *Journal of Geophysical Research*, *106*(C10), 22,277–22,294. https://doi.org/10.1029/2000JC000642

Smith, P. C. (1976). Baroclinic instability in the Denmark Strait overflow. *Journal of Physical Oceanography*, *6*(3), 355–371. https://doi.org/10.1175/1520-0485(1976)006\$<\$0355:BIITDS\$>\$2.0.CO;2

Spall, M. A., Pickart, R. S., Lin, P., von Appen, W.-J., Mastropole, D., Valdimarsson, H., et al. (2019). Frontogenesis and variability in Denmark Strait and its influence on overflow water. *Journal of Geophysical Research: Oceans*, *49*, 1889–1904. https://doi.org/10.1175/JPO-D-19-0053.1

Spall, M. A., & Price, J. F. (1998). Mesoscale variability in Denmark Strait: The PV out flow hypothesis. *Journal of Physical Oceanography*, *28*(8), 1598–1623. https://doi.org/10.1175/1520-0485(1998)028\$<\$1598:MVIDST\$>\$2.0.CO;2

Våge, K., Pickart, R. S., Spall, M. A., Valdimarsson, H., Jónsson, S., Torres, D. J., et al. (2011). Significant role of the North Icelandic Jet in the formation of Denmark Strait overflow water. *Nature Geoscience*, *4*, 723–727. https://doi.org/10.1038/ngeo1234

Voet, G., & Quadfasel, D. (2010). Entrainment in the Denmark Strait overflow plume by meso-scale eddies. *Ocean Science*, *6*(1), 301–310. https://doi.org/10.5194/os-6-301-2010

von Appen, W.-J., Mastropole, D., Pickart, R. S., Valdimarsson, H., Jónsson, S., & Girton, J. B. (2017). On the nature of the mesoscale variability in Denmark Strait. *Journal of Physical Oceanography*, *47*(3), 567–582. https://doi.org/10.1175/JPO-D-16-0127.1

von Appen, W.-J., Pickart, R. S., Brink, K. H., & Haine, T. W. (2014). Water column structure and statistics of Denmark Strait overflow water cyclones. *Deep Sea Research I*, *84*, 110–126. https://doi.org/10.1016/j.dsr.2013.10.007

Worthington, L. V. (1969). An attempt to measure the volume transport of Norwegian Sea over flow water. *Deep Sea Research*, *16*, 421–432.